Ultramicroscopy 110 (2010) 383–389

Contents lists available at ScienceDirect

Ultramicroscopy

journal homepage: www.elsevier.com/locate/ultramic

Dopant profiling of focused ion beam milled semiconductors using off-axis electron holography; reducing artifacts, extending detection limits and reducing the effects of gallium implantation

David Cooper [a,*], Cyril Ailliot [a], Jean-Paul Barnes [a], Jean-Michel Hartmann [a], Phillipe Salles [b], Gerard Benassayag [b], Rafal E. Dunin-Borkowski [c]

[a] CEA, LETI, MINATEC, F38054 Grenoble, France
[b] CEMES-CNRS, nMat group, 29 rue Jean Marvig, 31055 Toulouse, France
[c] Center for Electron Nanoscopy, Technical University of Denmark, DK-2800 Kongens Lyngby, Denmark

ARTICLE INFO

Keywords:
Dopant profiling
Off-axis electron holography
Focused ion beam milling

ABSTRACT

Focused ion beam (FIB) milling is one of the few specimen preparation techniques that can be used to prepare parallel-sided specimens with nm-scale site specificity for examination using off-axis electron holography in the transmission electron microscope (TEM). However, FIB milling results in the implantation of Ga, the formation of amorphous surface layers and the introduction of defects deep into the specimens. Here we show that these effects can be reduced by lowering the operating voltage of the FIB and by annealing the specimens at low temperature. We also show that the electrically inactive thickness is dependent on both the operating voltage and type of ion used during FIB milling.

1. Introduction

There is a need in the semiconductor industry for a characterisation technique that can be used to provide quantitative maps of dopants in microelectronic devices with nm-scale spatial resolution [1]. Off-axis electron holography is a transmission electron microscopy (TEM) technique that involves the use of an electron biprism to interfere an electron wave that has passed through a specimen with a reference wave that has passed through vacuum, to form an interference pattern or electron hologram. From the electron hologram, phase and amplitude images of the specimen can be reconstructed. As the phase is very sensitive to changes in electrostatic potential in the specimen, electron holography can in principle fulfil the industry requirements for active dopant mapping [2–7]. In the absence of diffraction contrast and magnetic fields, the phase change of an electron that has passed through a specimen is given by the expression

$$\Delta\phi = C_E \int_0^t V(x,y,z)\,dz, \tag{1}$$

where C_E is a constant dependent on the energy of the electron wave (7.29×10^{-3} rads V^{-1} nm^{-1} for 200 kV electrons), V is the electrostatic potential and z is the electron beam direction [8]. Therefore, it is important to know the electrically active thickness, t_{active} of a specimen if the phase images are to be converted into quantitative maps of the electrical potential in microelectronic devices.

The task of preparing a TEM specimen that contains an individual 30-nm-gate transistor from a 300 mm wafer has been made easier by the development of dual beam systems which combine the capabilities of field emission gun (FEG) scanning electron microscopes (SEMs) with focused ion beams (FIBs). They allow regions of interest to be identified quickly and thin parallel-sided membranes suitable for electron microscopy to be removed from the wafer and examined by TEM [9]. Many of the initial problems that have been associated with FIB milling have now been resolved, for example the use of low energy Ga ion beams to reduce the thicknesses of the amorphous surface layers [10] and the use of Ar ion milling to remove Ga implantation [11]. For medium resolution off-axis electron holography, a critical parameter is commonly referred to as the 'electrically inactive thickness' [12], which describes the combined effects of surface band-bending [13] and both implantation and damage introduced into the crystalline regions of specimens during ion milling [14]. This damage is caused by secondary collisions which occur deep in the crystalline regions of the specimens and introduce defects that can trap the charge carriers [15].

2. Experimental details

In order to assess the effects of FIB specimen preparation on the electrostatic potentials in semiconductors measured using

* Corresponding author.
E-mail addresses: david.cooper@cea.fr, daveycooper@gmail.com (D. Cooper).

0304-3991/$ - see front matter © 2010 Elsevier B.V. All rights reserved.
doi:10.1016/j.ultramic.2010.02.001

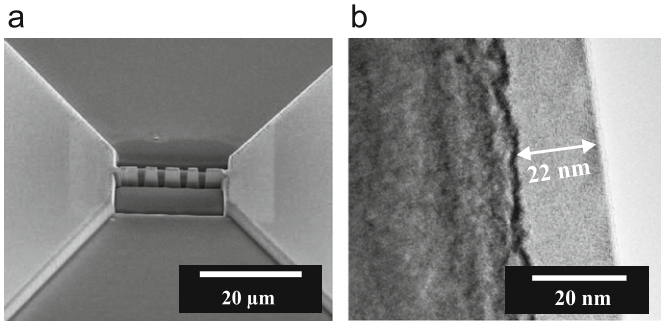

Fig. 1. (a) SEM image of a FIB-prepared specimen suitable for examination by electron holography. Five membranes of different thickness are present, each separated by an area of vacuum for providing a vacuum reference wave for electron holography. (b) High-resolution image of the edge of one of the specimens. An amorphous surface layer is present as well as damage in the crystalline region of the specimen.

off-axis electron holography, nominally abrupt Si *p*–*n* and *n*–*p* junction specimens containing symmetrical dopant concentrations were grown using reduced pressure chemical vapour deposition. For the *n*–*p* junctions, a 1.0 μm layer of phosphorus (*n*-type) doped Si was grown on a 1.0 μm layer of boron (*p*-type) doped Si on a lightly *p*-doped substrate. The inverse procedure was used for the *p*–*n* junctions. Samples were grown with nominal dopant concentrations of 2×10^{17}, 2×10^{18} and 1×10^{19} cm^{-3}, which were subsequently confirmed using secondary ion mass spectrometry (SIMS) [16].

TEM specimens were prepared using a FEI Strata Dual Beam FIB operated at different voltages. Before milling, the regions of interest on the wafer surfaces were protected from normal incidence Ga ions by sputtering a thin layer of platinum and then depositing several microns of tungsten using ion beam assisted deposition. Fig. 1(a) shows an SEM image of one of the TEM specimens prepared in the 'conventional' or 'H-Bar' FIB milling geometry. The specimen contains several membranes with a range of thicknesses between 150 and 500 nm. Multiple specimens were prepared from each wafer using FIB operating voltages of either 30 or 8 kV. Fig. 1(b) shows a high-resolution TEM image of the edge of one of the specimens prepared using 30 kV Ga ions. Both the amorphous surface layer and damage in the crystalline regions of the specimen can be seen.

Electron holograms were acquired of the *p*–*n* junctions using a FEI Titan FEGTEM operated at 200 kV. The holograms were recorded using a 2048×2048 pixel charge coupled device (CCD) camera with the objective lens of the microscope turned off and a Lorentz lens used to extend the field of view in each hologram to 1.5 μm by 700 nm. The interference fringe spacing was 3.5 nm which corresponds to a spatial resolution in the reconstructed phase images of approximately 10 nm. Although the spatial resolution in this operating mode can in principle be improved to $\sim$4 nm at the expense of fringe contrast and the number of counts recorded, in this experiment the settings were chosen to optimise the field of view. The mechanical and electrical stability of the Titan allowed individual electron holograms to be acquired for time periods of a minute or more, leading to reconstructed phase images with excellent signal-to-noise ratios [17].

3. The inactive layer in silicon

The inactive layer can be defined as the crystalline near-surface region in the specimens in which dopants are not electrically active [19]. In a doped semiconductor examined using off-axis electron holography, the phase is directly proportional to the specimen thickness, according to the expression

$$\Delta\phi = C_E V_{bi}(t_{cryst} - t_{inactive}). \quad (2)$$

The presence of an inactive layer then results in measured values of potential that are lower than expected in a bulk-like specimen. In this study the specimen thickness was measured using convergent beam electron diffraction (CBED) [18]. As CBED is sensitive only to the 'crystalline' contribution to the specimen thickness, these measurements automatically exclude the amorphous surface layers from the calculation of potentials from phase images.

It is in principle possible to recover the built-in potentials in doped semiconductors from the expression

$$\Delta\phi = C_E V_{bi} t_{active}, \quad (3)$$

where the electrically active thickness, $t_{active} = t_{cryst} - t_{inactive}$. It has been shown by performing 3D reconstructions of the phase measured in specimens containing simple *p*–*n* junctions that the inactive thickness is not abrupt [21].

This can also be seen in Fig. 2(a) where a reconstructed phase image of a 370-nm-thick specimen containing a *n*–*p* junction with a dopant concentration of 2×10^{18} cm^{-3} is shown. Although the differently doped regions can be distinguished, it is apparent from the phase image that the *p*–*n* junction does not extend to the edge of the specimen, which remains at the same potential as the *p*-type region. This can be seen more clearly in Fig. 2(b) which shows the cosine of the phase. Fig. 2(c) shows phase profiles measured across the junction averaged over 25 nm and at different distances, *d* from the edge of the specimen. Due to surface effects, the phase varies depending on the distance from the edge of the specimen where the profile is taken. The top and bottom surfaces of the specimen are likely to be damaged in a similar manner during FIB preparation. Fig. 2(d) and (e) show a corresponding amplitude image and a thickness map [20] of the specimen. No dopant related contrast can be seen in the amplitude image (the dopant concentration corresponds to one dopant atom to 25,000 Si atoms, or just 0.004%). The thickness profile shown in Fig. 2(f) shows that the specimen is flat and parallel-sided and that the contrast observed in the phase image in Fig. 2(a) is associated with changes in potential and not in thickness. The thickness is measured in units of mean free path. The mean free path in Si is dependent on the acceleration voltage of the electron beam as well as certain parameters used in the TEM such as the collection aperture.

Although the inactive thickness $t_{inactive}$ can in principle be quantified [19], care must be taken, both because it is not an abrupt surface layer and because its value depends on the dopant species and concentration. Fig. 3 shows the step in phase measured across a series of *p*–*n* junctions as a function of crystalline specimen thickness, t_{cryst}, for specimens with a dopant concentration of (a) 1×10^{17}, (b) 2×10^{18}, and (c) 1×10^{19} cm^{-3}. By making use of Eq. (2), an estimate of the inactive thickness can be obtained from the *x*-intercept of the graphs. These values are given for all of the different specimens in Table 1. The results show that the inactive thickness depends not only on the energy of the Ga ions that are used to prepare the specimen, but also on the dopant concentration, indicating that there is a complex relationship between measured phase and potential in specimens that have varying dopant concentrations, and that for quantitative dopant profiling the nature of the inactive thickness must be better understood. Fig. 3 also shows that the inactive thickness can be reduced by approximately a factor of two by reducing the operating voltage of the FIB from 30 to 8 kV. However, the damage is still significant and therefore, a reduction in the operating voltage of the FIB alone will not solve this problem. It is known

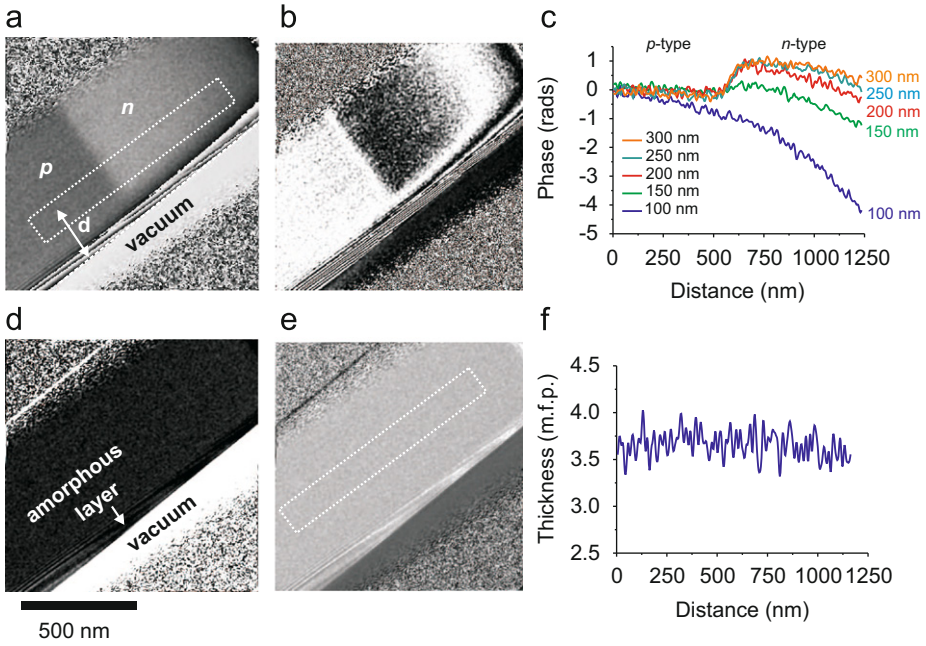

Fig. 2. (a) Phase image of a Si specimen with a measured crystalline thickness of 370 nm containing a n–p junction with a nominal dopant concentration of $2\times10^{18}\,cm^{-3}$. (b) Cosine of the phase. (c) Profiles extracted from across the phase image at different distances from the specimen edge. (d) and (e) Amplitude image and corresponding thickness map in units of mean free path, respectively. (f) Profile taken from the indicated region of the thickness map in units of mean free path.

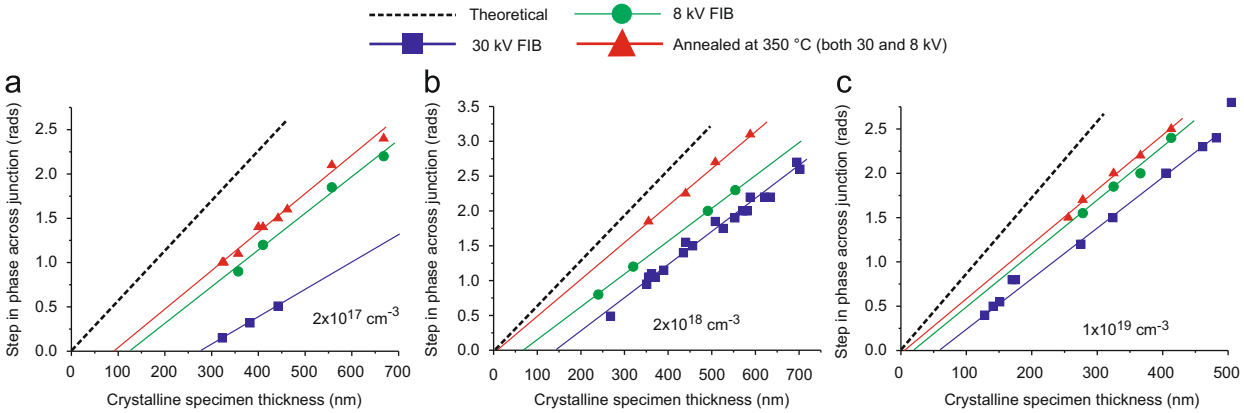

Fig. 3. Steps in phase measured across a series of symmetrical Si p–n junctions plotted as a function of crystalline specimen thickness for nominal dopant concentrations of (a) 2×10^{17}, (b) 2×10^{18} and (c) $1\times10^{19}\,cm^{-3}$. The specimens were prepared in the FIB operated at 30 or 8 kV. Data from specimens that were subsequently annealed at low temperature are also shown. The steps in phase that would be expected from theory (assuming no inactive surface layers) are shown using dashed lines.

Table 1
Electrically inactive thickness (in units of nm) measured for the differently doped Si specimens and different preparation methods. Annealed specimens obtained after using either 30 or 8 kV Ga ions provide the same results. The experimental error in each case is ±15 nm.

Dopant concentration (cm^{-3})	30 kV	8 kV	Annealed at 350 °C
1×10^{19}	60	25	5
2×10^{18}	140	60	10
2×10^{17}	250	130	85

that by annealing either Si or GaAs specimens at low temperature, defects that are introduced into the specimens during FIB milling can be removed and the inactive layer reduced [14]. Experimental data for Si specimens that have been annealed at only 320 °C are shown in Fig. 3. The resulting values of inactive thickness in Table 1 show that the inactive layer is reduced to below 10 nm for specimens with dopant concentrations of at least $2\times10^{18}\,cm^{-3}$, whereas it remains at 85 nm for specimens with dopant concentrations of $2\times10^{17}\,cm^{-3}$. This value of 85 nm could not be reduced either by preparing the specimens at lower energy in the FIB or by annealing the specimens for longer periods or at temperatures up to 500 °C. The specimens that were prepared using 30 or 8 kV Ga ions were found to have the same value of inactive thickness after annealing.

Fig. 4 shows the inactive thickness measured from the differently doped specimens plotted as a function of the FIB operating voltage. The specimens that were annealed are indicated as having been prepared using a FIB operated at zero kV. The intercept with the y-axis can be thought of as the electrically inactive thickness that would remain in a perfect

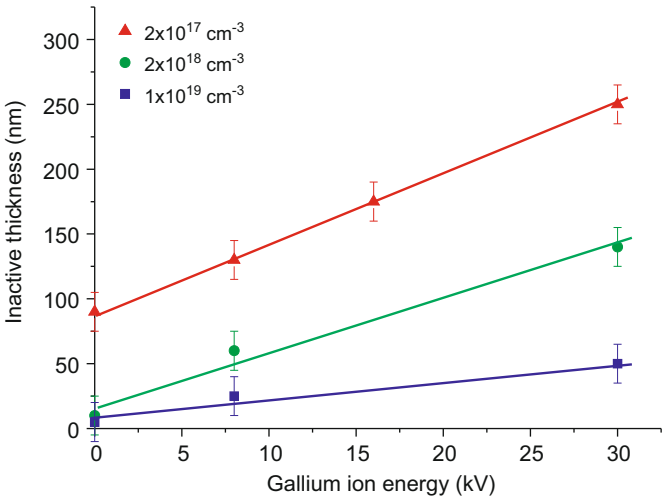

Fig. 4. Electrically inactive layer thickness in the differently doped Si specimens plotted as a function of FIB operating voltage. Annealed specimens are indicated as having been prepared using a FIB operated at zero kV.

crystalline TEM specimen due to surface depletion or band bending. Surface depletion in a thin TEM specimen can be affected by the formation of charged specimen surfaces due to secondary electron emission in the TEM [25,26]. It has been shown that the presence of this surface charge can in some semiconductor samples influence the lower-limit of dopant concentration that can be measured [13]. Therefore, when low dopant concentrations are present, care must be taken to account for possible artefacts that are introduced by the accumulation of surface charge during TEM examination.

4. Measuring the built-in potential

Eq. (2) suggests that the built-in potential V_{bi} across a p–n junction can be determined from the gradients of graphs such as those shown in Fig. 3 on the assumption that the inactive thickness is the same for each crystalline thickness. Both the theoretical and experimental results are shown in Table 2. The values of V_{bi} are not only much lower than predicted for bulk-like specimens [22] but are also independent of the FIB operating voltage used to prepare the specimens. Although annealing increases the measured values of V_{bi} by small amounts [14], they are still lower than expected.

Fig. 5 shows the values of V_{bi} across the junctions plotted as a function of dopant concentration. The experimental and theoretical values converge at higher dopant concentrations suggesting that for dopant concentrations above $3\times10^{19}\,\mathrm{cm}^{-3}$ it may be possible to recover the 'correct' built-in potential for Si p–n junction specimens if prepared using low energy ion milling to minimise the inactive thickness.

Previously published results suggest that the correct value of V_{bi} can be measured from a FIB-prepared Si or GaAs p–n junction if the region of interest on the specimen has an improved electrical connection to the microscope ground, for example by using an electrical biasing holder [19,23,27]. During the observation of a FIB-prepared GaAs p–n junction examined in this way, a specimen current of 500 μA was generated by exposure to the electron beam. The presence of such currents may influence potentials measured using electron holography. Experimental results shown elsewhere suggest that such problems can sometimes be avoided if wedge polishing is used with no additional Ar ion milling [24].

Table 2
Built-in potentials (in units of V) measured for the differently doped junction specimens, as compared with the values expected for bulk-like specimens from theory. The experimental error in each case is ±0.05 V.

Dopant concentration (cm^{-3})	Experimental	Theory
1×10^{19}	0.86	1.06
2×10^{18}	0.63	0.98
2×10^{17}	0.41	0.90

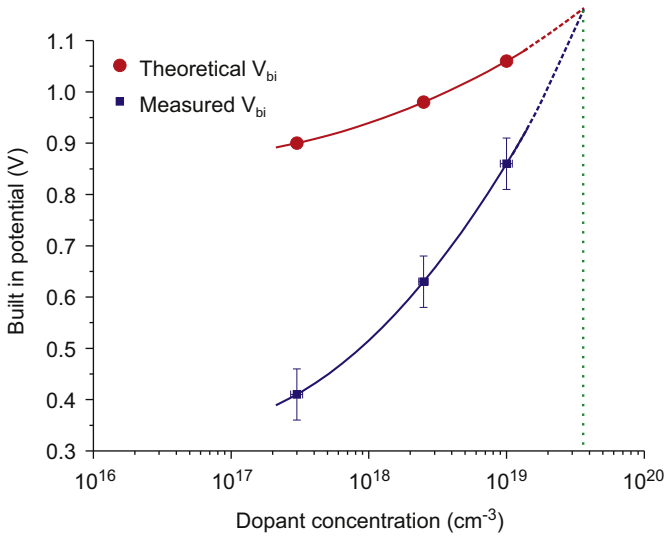

Fig. 5. Measured built-in potential plotted as a function of dopant concentration for experimental results acquired from different Si p–n junctions; shown alongside predictions for bulk-like devices.

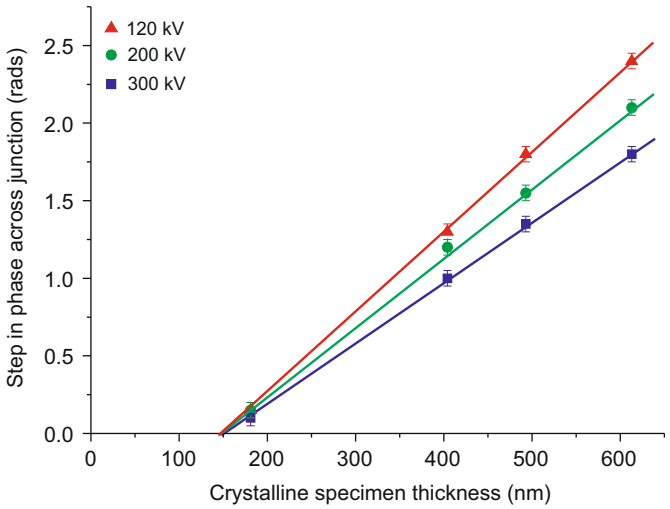

Fig. 6. Step in phase measured as a function of crystalline specimen thickness for a Si p–n junction with a dopant concentration of $2\times10^{18}\,\mathrm{cm}^{-3}$ examined using different microscope operating voltages.

5. The effect of microscope operating voltage

In order to assess if the energy of the electron beam influences measured potentials, a FIB-prepared symmetrical Si p–n junction

Table 3
Values of the constant C_E and the measured built-in potential, V_{bi} for each of the microscope acceleration voltages used, for a Si p–n junction specimen with a nominal dopant concentration of $2\times10^{18}\,cm^{-3}$. The experimental error in the values of V_{bi} is ±0.05 V.

Operating voltage (kV)	C_E (rads V^{-1} nm^{-1})	V_{bi} (V)
120	0.00856	0.60
200	0.00729	0.63
300	0.00653	0.60

specimen with dopant concentrations of $2\times10^{18}\,cm^{-3}$ was examined at accelerating voltages of 120, 200 and 300 kV. By lowering the operating voltage of the TEM, knock-on specimen damage from high-energy electrons may be reduced. However, the stronger interaction between the specimen and the electron beam may lead to increased charging [18]. Care was taken to ensure that the beam current was kept low and consistent between the different accelerating voltages. Fig. 6 shows the measured step in phase across the junctions plotted as a function of crystalline specimen thickness measured using CBED. As expected, a greater phase shift is measured as the accelerating voltage is reduced. The values of V_{bi} inferred from the 120, 200 and 300 kV measurements are shown in Table 3, and are consistent with each other within experimental error. The electrically inactive thickness is reproducibly 140 nm in each case. For the experiments performed here, the experimental results therefore appear to be independent of microscope operating voltage.

6. A note on gallium arsenide

Several articles have discussed electron holography experiments performed on GaAs samples containing p–n junctions [14,27–30], for example, it is known that the inactive layer in these p–n junctions is dependent on the operating voltage of the FIB [31]. However, no experimental results have been published to show whether the inactive thickness in GaAs also depends on the dopant concentration.

Electron holography was used to examine GaAs specimens containing p–n junctions that had been grown by molecular beam epitaxy. The specimens each comprised a 1.0-μm−thick Be-doped (n-type) layer grown on a 1.0-μm−thick, Si-doped (p-type) layer on a doped GaAs (0 0 1) substrate. Specimens with symmetrical dopant concentrations of 1×10^{17} and $1\times10^{18}\,cm^{-3}$ were prepared for TEM examination using a FIB operated at 30 kV and then examined using the experimental procedure described above for Si specimens. Fig. 7 shows the step in phase measured across the GaAs p–n junctions as a function of crystalline specimen thickness measured using CBED. From the x-intercept it is clear that, just as for Si, the inactive layer thickness is strongly dependent on dopant concentration. Table 4 shows the values of inactive thickness measured for the GaAs specimens. As only two different specimens were examined, further detailed analysis was not carried out here. However, it is clear that care must be taken when measuring potentials in GaAs semiconductors that have varying dopant concentrations. The theoretical values of V_{bi} for bulk-like GaAs are 1.33 and 1.38 V for dopant concentrations of 1×10^{17} and $1\times10^{18}\,cm^{-3}$, respectively. Experimentally, values of 0.53 and 0.96 V are measured. It has previously been shown that for these GaAs specimens the predicted value of V_{bi} could be obtained by improving the electrical contacts to the region of interest on the specimen [27]. The behaviour of these GaAs p–n junctions appears to be similar to that seen in Si p–n junctions specimens with similar dopant concentrations.

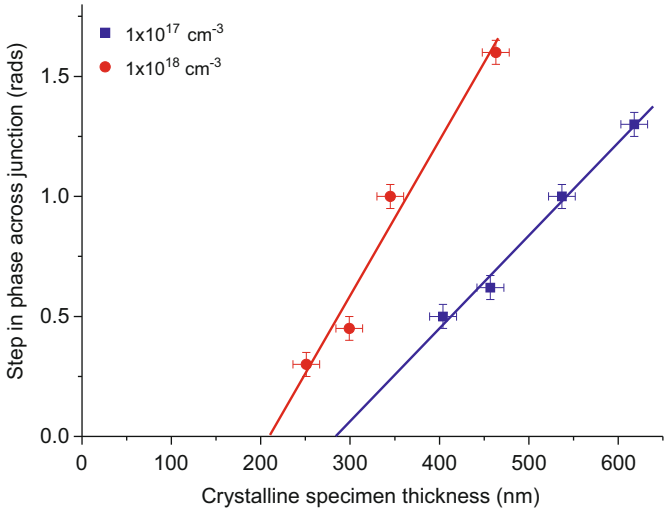

Fig. 7. Steps in phase across GaAs specimens containing p–n junctions plotted as a function of crystalline specimen thickness for nominal dopant concentrations of 1×10^{17} and $1\times10^{18}\,cm^{-3}$.

Table 4
Electrically inactive thicknesses and built-in potentials measured for GaAs p–n junctions.

Dopant concentration (cm^{-3})	Inactive thickness (nm)	V_{bi} (V)
1×10^{18}	210 ± 15	0.96 ± 0.1
1×10^{17}	270 ± 15	0.53 ± 0.1

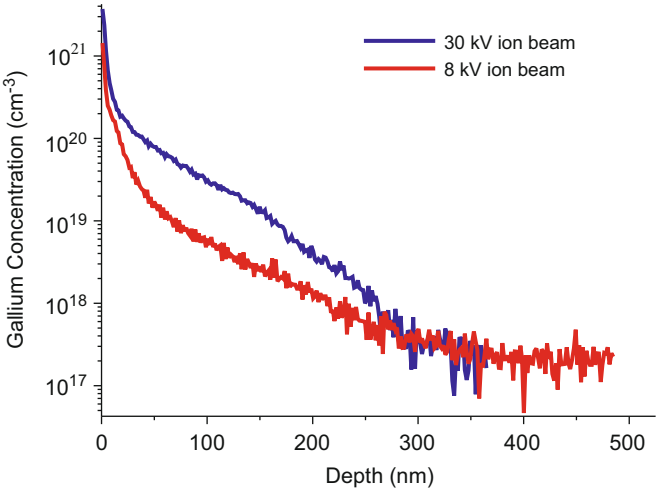

Fig. 8. SIMS profiles of Ga content in bulk Si. Test structures were prepared using both 30 and 8 kV ions.

7. Specimen preparation using focused silicon ions

A key problem with FIB milling is that of ion implantation, especially since Ga acts as a dopant in Si. SIMS was performed on FIB-milled Si test samples in order to assess the depth and concentration of Ga ions, using either 30 or 8 kV Ga ions. Currents of 10 nA were used to mill areas of 100 μm^2 suitable for analysis by Time of Flight (ToF) SIMS at the side of a Si bar using the same method that would be used to prepare a TEM specimen in the H-Bar geometry. An angle of incidence of 1° relative to the side of the specimen was used. ToF

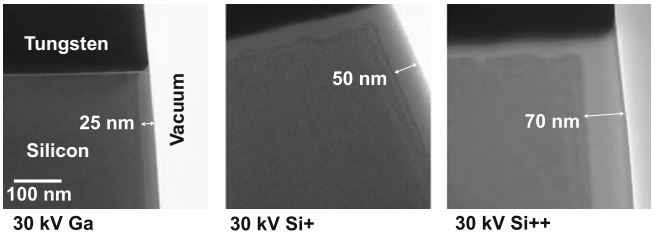

Fig. 9. High-resolution TEM bright-field images showing amorphous surface layers on Si specimens prepared using 30 kV Ga, Si^+ and Si^{++} ion beams.

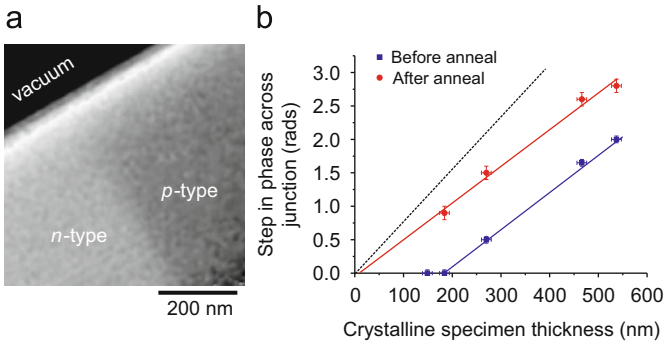

Fig. 10. (a) Phase image acquired from a 450-nm-thick Si specimen containing a p–n junction prepared using a 30 kV Si^+ ion beam. The extent of the inactive layer thickness can be seen at the specimen edge. (b) Phase shifts across p–n junctions plotted as a function of crystalline specimen thickness both before and after annealing.

SIMS dual beam depth profiles were performed using a ToF SIMS 5 instrument from ION ToF GmbH. Sputtering was performed using a 500 eV O_2^+ beam scanned over a $250 \times 250\,\mu m^2$ area, whilst analysis was performed using a Bi^+ ion beam at 25 keV scanned over a $60 \times 60\,\mu m^2$ area. The two ion beams were centred on the FIB-milled area. An oxygen partial pressure of 1.5×10^6 mbar was used during analysis. Fig. 8 shows the SIMS profiles obtained for the different FIB operating voltages. Although the Ga concentrations measured here appear to be extremely high, they are in agreement with atom probe data, which show that a Ga concentration of 1% is present at a depth of ~50 nm [32]. The depth measurement of Ga implantation may be influenced by Ga remaining in the sidewalls of the FIB-milled areas of the specimen. However, these results suggest that high concentrations of Ga are present in crystalline Si regions as well as in the amorphous surface layers of the specimen and ideally these should be removed.

In order to prepare specimens without Ga implantation, Si p–n junctions with dopant concentrations of $2 \times 10^{18}\,cm^{-3}$ were milled to a thickness of 2 μm using conventional FIB milling and then thinned to range of thicknesses between 100 and 500 nm using an ExB Orsay Physics SiAu liquid metal source [33]. An energy filter was used to select the ions, and specimens were prepared using both Si^+ and Si^{++} beams. Final milling was performed using beam currents of ~20 pA. Fig. 9 shows high-resolution TEM bright field images which illustrate that the amorphous layer thicknesses are 25, 50 and 70 nm for specimens prepared using 30 kV Ga, Si^+ and Si^{++} ion beams, respectively. This trend is expected, as Si ions have a much larger range than the Ga ions in Si specimens.

Electron holograms were acquired from specimens using the procedure as described above. Fig. 10(a) shows a phase image acquired from a 450-nm-thick Si specimen containing a $2 \times 10^{18}\,cm^{-3}$ p–n junction, prepared using Si^+ ions. The presence of an inactive specimen surface layer is apparent as the junction contrast disappears ~250 nm from the specimen edge. Fig. 10(b) shows phase shifts measured across a series of p–n junctions plotted as a function of crystalline specimen thickness. Before annealing, the inactive thickness is 170 ± 15 nm. Whereas an annealing temperature of 320 °C did not improve the results, a 30 min anneal at 450 °C reduced the inactive thickness to 10 ± 15 nm. (There is a possibility that the required temperature of the anneal resulted from poor thermal contact between the specimen and the heating holder.)

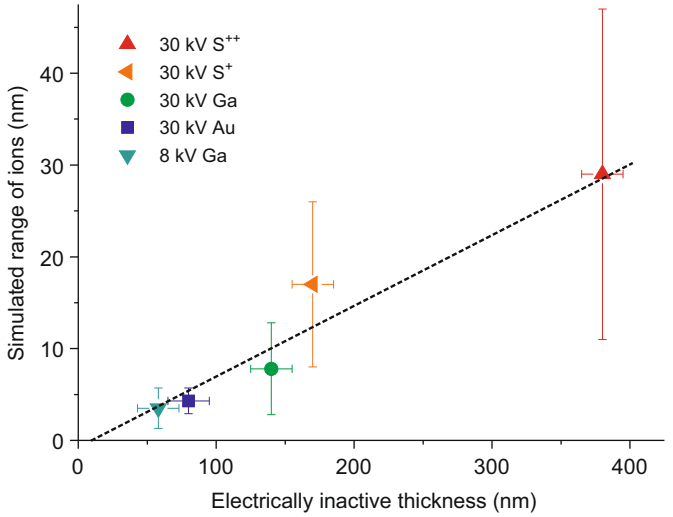

Fig. 11. Simulations of the ion ranges plotted as a function of inactive layer thickness measured in a Si p–n junction with a dopant concentration of $2 \times 10^{18}\,cm^{-3}$. The error bars for the ranges of the ions are taken from the ion straggle.

For the p–n junctions prepared using the Si^{++} ions with a range of final specimen thicknesses of 140–380 nm, the junction was not detected in any of the specimens except the 380-nm-thick membrane where dopant contrast was just detected.

By using light ions such as Si, the amorphous surface layers and subsequent electrical damage within the specimen are much greater than for heavier ions such as Ga. Therefore, in order to use Si ions to prepare specimens for TEM analysis, it would be preferable to use low accelerating voltages in the FIB. Such experiments will be performed in the near future.

In order to better understand the effects of ion energy on the inactive layer thickness, simulations of the ion range in silicon were performed using SRIM [34]. The ions were assumed to have a grazing incidence of 1°, and their range was plotted as a function of inactive thickness measured in specimens with a dopant concentration of $2 \times 10^{18}\,cm^{-3}$. Data obtained previously using 30 kV Au ions were included in the comparison [33]. As Au ions have a greater mass than Ga ions, the inactive thickness is smaller than observed for Ga.

Fig. 11 shows the ion range plotted as a function of inactive thickness for Si p–n junctions with a dopant concentration of $2 \times 10^{18}\,cm^{-3}$. The inactive thickness clearly follows the trend predicted by the SRIM simulations. The x-intercept predicts a residual inactive thickness of 15 ± 15 nm in undamaged specimens, which is consistent with the value measured in annealed specimens.

Values of inactive thickness for other ions can be predicted from Fig. 11. For example, Ar milling is routinely used to prepare specimens for examination using off-axis electron holography [35]. SRIM simulations for 3 kV Ar ions at an angle of incidence of 5° predict an ion range of 2.5 nm. From Fig. 11, this value corresponds to an inactive thickness of 40 nm in specimens with a dopant concentration of $2 \times 10^{18}\,cm^{-3}$, and to a significantly larger value in specimens with lower concentrations.

The simulations also show that by using 1 kV Ga ions at a grazing angle of incidence, the ion range is 1.1 nm, corresponding to an inactive thickness of approximately 15 nm. This suggests that by

using very low energy Ga ions, the inactive thickness due to specimen damage is similar to that observed due to surface band bending alone. Therefore, there is a possibility that if parallel-sided specimens can be prepared using very low energy ion milling (or other heavy ions such as Au or Xe), then the annealing stage may not be necessary.

8. Conclusion

In this paper, artefacts that are observed in symmetrical Si *p–n* junction specimens that have been prepared using FIB milling and examined using off-axis electron holography have been discussed. FIB milling creates both an amorphous surface layer and an inactive crystalline layer, which is caused by physical damage to the crystalline regions of the specimens and by the build-up of charge on the specimen surface layers. The electrically inactive layer thickness in such specimens is dependent both on the ion species and energy used during specimen preparation and on dopant concentration.

In situ annealing of specimens containing *p–n* junctions to reduce damage in the crystalline regions of the specimens results in a small residual electrically inactive layer thickness for dopant concentrations above $2\times10^{18}\,\mathrm{cm}^{-3}$. However, an inactive thickness of 85 nm is still present in specimens with dopant concentrations of $2\times10^{17}\,\mathrm{cm}^{-3}$ even after annealing. It is unlikely that annealing will modify the dopant distribution in the semiconductor samples as low temperatures are used in comparison with those used in device processing. The annealing stage may be unnecessary for specimens that contain high dopant concentrations that are prepared carefully using low energy milling. Although the lower limit for the dopant concentration that can be detected can be extended by preparing TEM specimens using lower ion energies, surface charging rather than microscope performance may ultimately determine the lowest dopant concentration that can be observed [13]. Although the present work has focused on the problems that are associated with using ion milling to make specimens for examination by electron holography, it is interesting to note that experimental results published elsewhere suggest that wedge polishing alone may provide quantitative results [3,4,24,35].

The results shown here have suggested that the effects of specimen damage during ion milling and the build up of charge becomes less critical when high dopant concentrations are present. As modern semiconductor devices contain dopant concentrations as high as $5\times10^{20}\,\mathrm{cm}^{-3}$ implanted into lightly doped substrates, the problems that are discussed here may become less critical, especially if specimen preparation is well controlled. However, possible artefacts should still be considered, especially when examining interfaces between highly and lightly doped regions in device samples.

Acknowledgements

This work has been funded by the French RTB programme. We thank Ian Farrer from the University of Cambridge for providing the GaAs *p–n* junctions.

References

[1] International Technology Roadmap for Semiconductors, 2008 update. (Semiconductor Industry Association, San Jose, CA, 2008); ⟨http://public.itrs.net⟩.
[2] W.D. Rau, P. Schwander, F.H. Baumann, W. Hoppner, A. Ourmazd, Phys. Rev. Lett. 82 (1999) 2614–2617.
[3] M.A. Gribelyuk, M.R. McCartney, J. Li, S. Murthy, P. Ronsheim, B. Doris, J.S. McMurray, S. Hegde, D.J. Smith, Phys. Rev. Lett. 89 (2002) 025052.
[4] M.A. Gribelyuk, A. Domenicucci, P.A. Ronsheim, J.S. McMurray, O. Gluschenov, J. Vac. Sci. Technol. B 26 (2008) 408.
[5] A.T. Tilke, A. Lenk, U. Muhle, C. Wagner, C. Dahl, H. Lichte, IEEE Trans. Electron Dev. 52 (2005) 1067–1071.
[6] H. Lichte, P. Formanek, A. Lenk, M. Linck, C. Matzeck, M. Lehmann, P. Simon, Annu. Rev. Mater. Res. 37 (2008) 539–588.
[7] H. Lichte, Ultramicroscopy 108 (2008) 256–262.
[8] M.R. McCartney, D.J. Smith, Annu. Rev. Mater. Res. 37 (2008) 729–767.
[9] M.H.F. Overwijk, F.C. van den Heuval, C.W.T. Bulle-Lieumwa, J. Vac. Sci. Technol. B 11 (1993) 2021–2024.
[10] N.I. Kato, Y. Kohno, H. Saka, J. Vac. Sci. Technol. A 17 (1999) 1201–1204.
[11] A. Barna, B. Pecz, M. Menyhard, Ultramicroscopy 70 (1998) 161–171.
[12] A.C. Twitchett, R.E. Dunin-Borkowski, R.J. Hallifax, R.F. Broom, P.A. Midgley, J. Microsc. 214 (2003) 287.
[13] D. Cooper, P. Rivallin, J.-M. Hartmann, A. Chabli, R.E. Dunin-Borkowski, J. Appl. Phys. 106 (2009) 064506.
[14] D. Cooper, A.C. Twitchett, P.K. Somodi, I. Farrer, D.A. Ritchie, P.A. Midgley, R.E. Dunin-Borkowski, Appl. Phys. Lett. 88 (2006) 063510.
[15] PM. Mooney, L.J. Cheng, M. Suli, J.D. Gerson, J.W. Corbett, Phys. Rev. B 15 (1977) 3836.
[16] D. Cooper, C. Ailliot, R. Truche, J. Hartmann, J. Barnes, F. Bertin, J. Appl. Phys. 104 (2008) 064513.
[17] D. Cooper, R. Truche, P. Rivallin, J. Hartmann, F. Laugier, F. Bertin, A. Chabli, Appl. Phys. Lett. 91 (2007) 143501.
[18] D.B. Williams, C.B. Carter, Transmission Electron Microscopy, Plenum Press, New York, 1996.
[19] A.C. Twitchett, R.E. Dunin-Borkowski, R.J. Hallifax, R.F. Broom, P.A. Midgley, Phys. Rev. Lett. 88 (2002) 2383021.
[20] M.R. McCartney, M. Gajdardziska-Josifovska, Ultramicroscopy 53 (1994) 283–289.
[21] A.C. Twitchett, T. Yates, S.B. Newcomb, R.E. Dunin-Borkowski, P.A. Midgley, Nanoletters 7 (2007) 2020.
[22] S.M. Sze, Semiconductor Devices, Physics and Technology, Wiley, New York, 2002, pp. 180–184.
[23] D. Cooper, B. Aventurier, F. Templier, A. Chabli, Appl. Phys. Lett. 93 (2008) 183509.
[24] M.R. McCartney, M.A. Gribelyuk, J. Li, P. Ronsheim, J.S. Murray, D.J. Smith, Appl. Phys. Lett. 80 (2002) 3213–3215.
[25] M. Bellegia, P.F. Fazzini, P.G. Merli, G. Pozzi, Phys. Rev. B 67 (2003) 045328.
[26] P.F. Fazzini, P.G. Merli, G. Pozzi, F. Ubaldi, Phys. Rev. B 72 (2005) 085312.
[27] D. Cooper, A.C. Twitchett, P.A. Midgley, R.E. Dunin-Borkowski, J. Appl. Phys. 101 (2007) 094508.
[28] D. Cooper, R. Truche, A.C. Twitchett, P.A. Midgley, R.E. Dunin-Borkowski, J. Microsc. 223 (2009) 102–113.
[29] H. Sasaki, K. Yamamato, T. Hiriyama, S. Ootomo, T. Matsuda, R. Nakasaki, H. Ishii, Appl. Phys. Lett. 89 (2009) 244101.
[30] S. Chung, S. Johnson, Y. Zhang, D.J. Smith, M.R. McCartney, J. Appl. Phys. 105 (2009) 014910.
[31] D. Cooper, R. Truche, J.-L. Rouviere, Ultramicroscopy 108 (2008) 488–493.
[32] K. Thompson, D. Lawrence, D.J. Larsson, J.D. Olson, T.F. Kelly, B. Gorman, Ultramicroscopy 107 (2007) 131–139.
[33] D. Cooper, F. Bertin, P. Salles, G. Benassayag, Appl. Phys. Lett. 93 (2008) 043510.
[34] J.F. Zeigler, The Stopping and Range of Ions in Matter ⟨www.srim.org⟩, 2003.
[35] M.G. Han, P. Fejes, Q. Xie, S. Bagchi, B. Taylor, J. Connor, M.R. McCartney, IEEE Trans. Electron Dev. 54 (2007) 3336–3341.